analytical chemistry

pubs.acs.org/ac Letter

Structural Characterization of Individual α-Synuclein Oligomers Formed at Different Stages of Protein Aggregation by Atomic Force Microscopy-Infrared Spectroscopy

Lei Zhou and Dmitry Kurouski*

Cite This: https://dx.doi.org/10.1021/acs.analchem.0c00593 Read Online

ACCESS | Metrics & More | Article Recommendations | Supporting Information

ABSTRACT: Aberrant α-synuclein aggregation is strongly associated with the onset and development of Parkinson's disease (PD). Therefore, characterizing the structure of toxic intermediate oligomers plays an essential role in better understanding their neurotoxicity. Using atomic force microscopy-infrared spectroscopy (AFM-IR), we were able to reveal the structure of α-synuclein oligomers present at different stages of protein aggregation and establish a relationship between morphology and structure on the single oligomer level. We were also able to probe the secondary structure evolution of individual oligomers. Moreover, the IR spectra of individual oligomers suggest structural rearrangement that is necessary for oligomers with an antiparallel β-sheet to propagate into fibrils that have a parallel-β-sheet secondary structure. Detailed investigation of structural organization of α-synuclein oligomers reported in this study is critically important to understand the toxicity of these protein species. We also anticipate that this work will help developing approaches for oligomer detection and consequently presymptomatic diagnostic of PD.

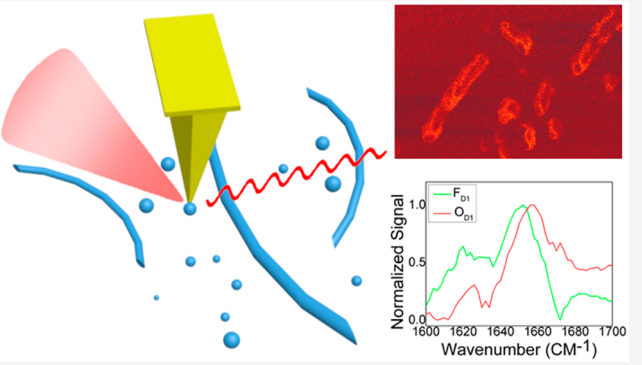

Around 6 million people are living with Parkinson's disease (PD) worldwide.[1] Postmortem examination of brains of people with PD revealed the presence of amyloid plaques, extracellular protein deposits that were associated with neuron degradation.[2] Similar histological evidence has been observed for other neurodegenerative maladies, such as Alzheimer's[3] and Huntington's[4] diseases. A large variety of physical and analytical methods, such as X-ray crystallography[5,6] and cryo-electron microscopy (cryo-EM),[7,8] were used to reveal the structural organization of amyloid aggregates. It has been found that fibrils were mainly made up of ordered β-sheet conformation.[9−11]

At the same time, there is very little known about oligomeric species that precede the formation of fibrils.[12] Experimental evidence suggests that oligomers exhibit much higher cell toxicity than fibrils.[13,14] However, the structural characterization of oligomers is extremely challenging because of their intrinsic instability. Chromatographic purification of oligomers typically results in the separation of only several of the most stable species that may only partially represent the structural diversity of these transient species.[15] The utilization of organic molecules such as curcumin[16] and baicalein[15] can inhibit the propagation of oligomers into fibrils. However, these organic molecules can also change the structure of oligomers. Moreover, there are many intermediate structures formed during the growth process as well as the initial monomers and final products, and most of the species are at the nanometer scale, which makes the study of these heterogeneous mixtures more challenging.[17] Although a wealth of information about the morphological diversity of oligomeric species has been obtained by cryo-EM examination,[18−20] the oligomers' heterogeneity limited an application of cryo-EM.

Atomic force microscopy-infrared spectroscopy (AFM-IR) offers a unique opportunity to solve this problem without a substantial sacrifice of sensitivity and spatial resolution of cryo-EM.[17,21−23] AFM-IR is capable of providing chemical information about the sample surface with subdiffraction limit spatial resolution.[24] AFM-IR has been utilized to investigate various topics in biology and surface chemistry including protein aggregates,[17,25,26] plant epicuticular waxes,[27] polymers,[28] and polycrystalline perovskite films.[29]

In this study, we report a detailed structural characterization of individual α-synuclein oligomers using AFM-IR (Scheme 1). α-Synuclein is a small (14 kDa) cytosolic protein that is enriched in presynaptic terminals. It has been observed that

Received: February 11, 2020
Accepted: April 29, 2020
Published: April 29, 2020

https://dx.doi.org/10.1021/acs.analchem.0c00593
Anal. Chem. XXXX, XXX, XXX−XXX

Scheme 1. Schematic Diagram Showing the Experimental Setup of AFM-IR

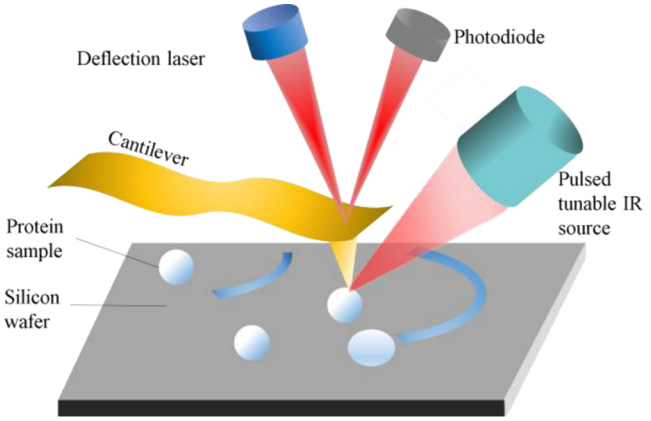

under physiological conditions, α-synuclein will aggregate forming small oligomers that further propagate into filaments, protofibrils, and fibrils. Such aberrant α-synuclein aggregation is strongly associated with the onset and development of PD. Using AFM-IR, we followed aggregation of α-synuclein and probed the structural organization of individual oligomers present at different stages of protein aggregation. We were able to establish a relationship between the structure and morphology on the single oligomer level. Our results also show the high structural heterogeneity of α-synuclein oligomers. We found that in the early stages of aggregation oligomers with an α-helix/random coil, parallel and antiparallel β-sheet secondary structures were formed. However, in late stages, we observed aggregates with dominating parallel β-sheet secondary structures and a small content of α-helix/random coil, whereas very little species with antiparallel β-sheet secondary structure were detected. These findings suggest the necessary rearrangement of antiparallel to parallel β-sheet secondary structures on the level of α-synuclein oligomers that is necessary for their propagation into fibrils.

RESULTS AND DISCUSSION

Morphology Characterization and Nanoscale IR Mapping of α-Synuclein Aggregates. AFM imaging was used to monitor the morphological evolution of α-synuclein with different incubation times (Figure S1). Before incubation (D0), most of the α-synuclein proteins presented as monomers with a height of approximately 1 nm (Figure S1A,F,K). After 1 day (D1) incubation, oligomers with various shapes and forms were present, most of them had spherical appearance, and some exhibited elongated topologies with a height centered at 6−8 nm (Figure S1B,G,L). In addition to spherical oligomers, we also observed the presence of protofilaments with similar heights of monomers. Similar spherical oligomeric species have also been observed at day 2 (D2) and day 3 (D3) as well as the protofibrils and possibly short fibrils of α-synuclein aggregation (Figure S1C,D). We found that at day 7 (D7), nearly all aggregates have fibril-like appearance, whereas a few oligomers were observed (Figure S1E).

Using the AFM-IR technique, we can also visualize the distribution of protein secondary structures in individual protein aggregates at all stages of α-synuclein aggregation. AFM images and the corresponding IR chemical maps at 1624 and 1655 cm^{-1} (Figures S2−S5) were taken at different incubation times. The 1655 cm^{-1} band has been widely accepted to be associated with random coil and α-helical conformations, while 1624 cm^{-1} is related to β-sheet conformation (Table S1). Overlapping of these two IR maps (Figure 1) was conducted to better demonstrate the structural

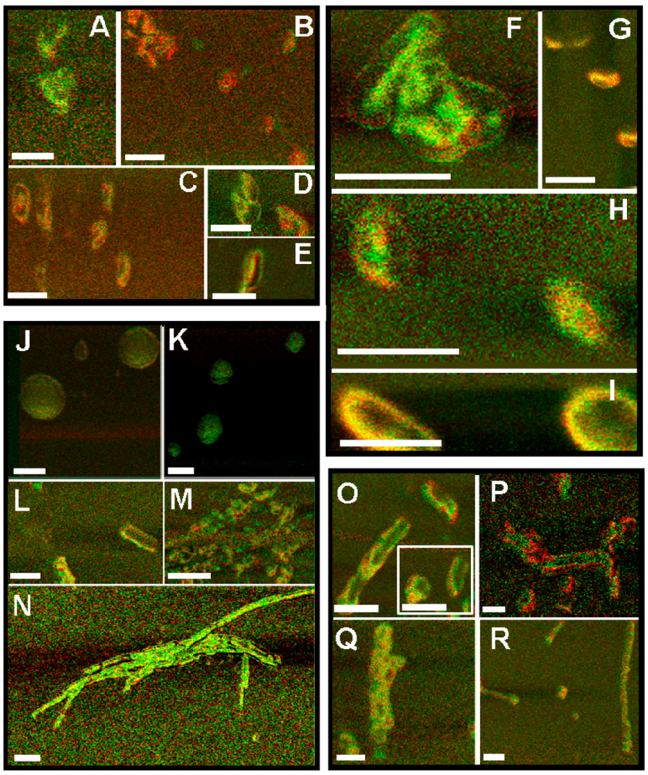

Figure 1. Overlapped infrared chemical maps at 1655 and 1624 $cm^{-1}$of D1 (A−E), D2 (F−I), D3 (J−N), and D7 (O−R) samples. Random coil and α-helical conformations (1655 cm^{-1}) and β-sheet (1624 cm^{-1}) are marked by pseudocolor red and green, respectively. Scale bars: A−I and O−R, 100 nm; J−N, 250 nm.

distribution of these aggregates. From a structural perspective, around half of all detected oligomers at D1 were dominated by the α-helix/random coil secondary structure (Figure 1B−D). In comparison, D2 oligomers exhibited much less α-helix/random coil secondary structure (Figure 1F−I), whereas the β-sheet content substantially increased. Figure 1F shows that some of these aggregates had a clearly visible β-sheet core. AFM-IR analysis of D3 aggregates showed clear evidence of the development of fibrils (Figure 1L). Besides that, we have also observed two types of spherical oligomers at D3: one showed close content of the β-sheet and α-helix/random coil secondary structures (Figure 1J) and the other primarily built by the β-sheet (Figure 1K). Moreover, the structural analysis of the formed fibrils on D3 showed a β-sheet-rich secondary structure (Figure 1N). One can expect that such high structural heterogeneity of α-synuclein oligomers should result in diverse mature fibrils. Indeed, nanoscale IR imaging revealed that α-synuclein aggregates at D7 were still heterogeneous from a perspective of the distribution of protein secondary structures. Although most of them had clearly a distinct β-sheet core (Figure 1O−P) surrounded by α-helix/random coil secondary structures, some of the observed D7 aggregates were composed of numerous smaller oligomers (Figure 1Q,R) packed in a side-by-side manner.

https://dx.doi.org/10.1021/acs.analchem.0c00593
Anal. Chem. XXXX, XXX, XXX−XXX

Nanoscale IR analysis not only offers an opportunity to probe the structural distribution of individual aggregates but can also hold the potential to monitor the IR absorption intensity quantitatively. By collecting spectra on protein aggregates, we found that α-synuclein underwent an increase in the β-sheet secondary structure (up to 75%) as the aggregation proceeded from D0 to D7 (Figure S6). Interestingly, though the overall β-sheet (parallel β-sheet (1624 cm^{-1}) and antiparallel β-sheet (1695 cm^{-1})) content is increasing along the aggregation process, the antiparallel β-sheet structures have detected an obvious increase at D1 and a gradual decrease at D2 and D3. In comparison, attenuated total reflection-Fourier-transformed infrared spectroscopy (ATR-FTIR, Figure S7) and circular dichroism (CD) spectra (Figure S6F) are much less sensitive than AFM-IR technique in terms of intermediate secondary structures, such as the antiparallel β-sheet (see the details in Figures S6 and S7).

Heterogeneity of α-Synuclein Oligomers. One may wonder whether this exclusive strength of AFM-IR can be used to visualize the structural heterogeneity of individual α-synuclein aggregates present at the same time point of protein aggregation. It can be seen that regardless of their significant difference in morphology, the secondary structure distribution also varies a lot (Figure S8). Furthermore, our results demonstrate that four different oligomers with similar morphology observed at D1 exhibited substantially different secondary structures (Figure 2). We found that oligomer 1 was

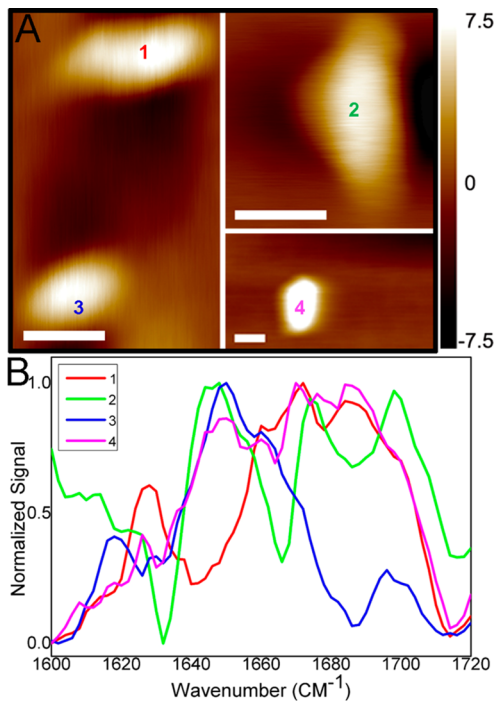

Figure 2. AFM images (A) and infrared spectra (B) of oligomers at D1. Scale bars, 50 nm.

primarily composed of a β-sheet (1624 cm^{-1}), β-turn (1675 cm^{-1}), and antiparallel β-sheet (1695 cm^{-1}) protein secondary structures, whereas a vibrational band that originates from a random coil/α-helix (~1650 cm^{-1}) has been observed in the spectra collected from oligomers 2, 3, and 4. Noticeably, the amount of antiparallel β-sheet (1695 cm^{-1}) was lower in oligomer 3 relative to others. Oligomers 2 and 4 appeared to have nearly equal intensities of vibrational bands that represent a random coil/α-helix (~1650 cm^{-1}) and β-turn (1675 cm^{-1}), suggesting the presence of all of these elements in its structure. It should be noted that morphologically, all of these oligomers were nearly indistinguishable. Thus, spectroscopic analysis is critically important to reveal the structural heterogeneity of the protein oligomers.

Structural Characterization of Spherical Oligomers and Fibrillar Aggregates. To better understand the distribution of parallel and antiparallel β-sheet structures, we acquired IR maps at 1624 and 1695 cm^{-1} for the D1, D2, and D7 samples (Figure 3). We found that at D1, most of the protofilaments exhibited a higher signal at 1624 cm^{-1} (parallel β-sheet) than the spherical counterparts (Figure 3B), whereas at 1695 cm^{-1} (antiparallel β-sheet), spherical ones had higher signals (Figure 3C).

To quantitatively analyze the distribution of parallel (1624 cm^{-1}) and antiparallel (1695 cm^{-1}) structures on these aggregates, spectra on protofilaments and spherical species (Figure 3E) were acquired and 1624 cm^{-1}/1695 cm^{-1} intensity ratio maps were conducted. As shown in Figure 3D, the protofilaments at D1 have a higher parallel/antiparallel ratio than spherical counterparts, which clearly indicate that the protofilaments have a higher parallel β-sheet content than antiparallel β-sheet. A similar trend had been observed at D2 (Figure 3I,J) and D7 (Figure 3N,O) when the protofibrils and fibrils are formed. Besides, our results suggest that spherical aggregates present at D1, D2, and D7 (Figure 3E,J,O) exhibit a similar structure, which are composed of a β-sheet (1624 cm^{-1}, 1695 cm^{-1}), α-helix/unordered (1663 cm^{-1}), and β-turn (1675 cm^{-1}) protein secondary structures. It indicates that the structure of the spherical aggregates remains similar along the fibrillar formation process except the gradual increasing of the parallel β-sheet structure at D2 and D7. The distinctly different secondary structures of the spherical aggregates and fibrillar ones indicate that the spherical aggregates should undergo structural rearrangement before growing into fibrils. The gradual increase of the parallel β-sheets structure in the spherical aggregates also indicates that they have a tendency to rearrange structures, though the rate is slow. Based on the above findings, we can also infer that those spherical aggregates need to be transformed into the parallel β-sheet rich structure rather than the antiparallel β-sheet rich structure in order to form fibrils.

It is expected that the secondary structure may change during sample drying. Since all of our IR (both AFM-IR and ATR-FTIR) measurements were conducted on dried sample, it would be of great importance to predict their corresponding solution-based secondary structure. Using synchrotron radiation circular dichroism (SRCD), Yoneda et al. found the secondary structure of the globular proteins exhibits only minor changes upon removal of bulk water during film formation, except the increase of the ordered structure.[30] Besides, Ramer et al. studied the AFM-IR spectra of diphenylalanine fibrils in water and in air, and they found that they show a high degree of similarity along the whole protein fingerprint spectral range.[26] These findings indicate that dried films has little influence on the secondary structure and can serve as a useful approach to examine the structure of proteins.

Morphological characterization and structural analysis of intermediate species formed during protein aggregation on a single-particle level are critically important to understand the

https://dx.doi.org/10.1021/acs.analchem.0c00593
Anal. Chem. XXXX, XXX, XXX−XXX

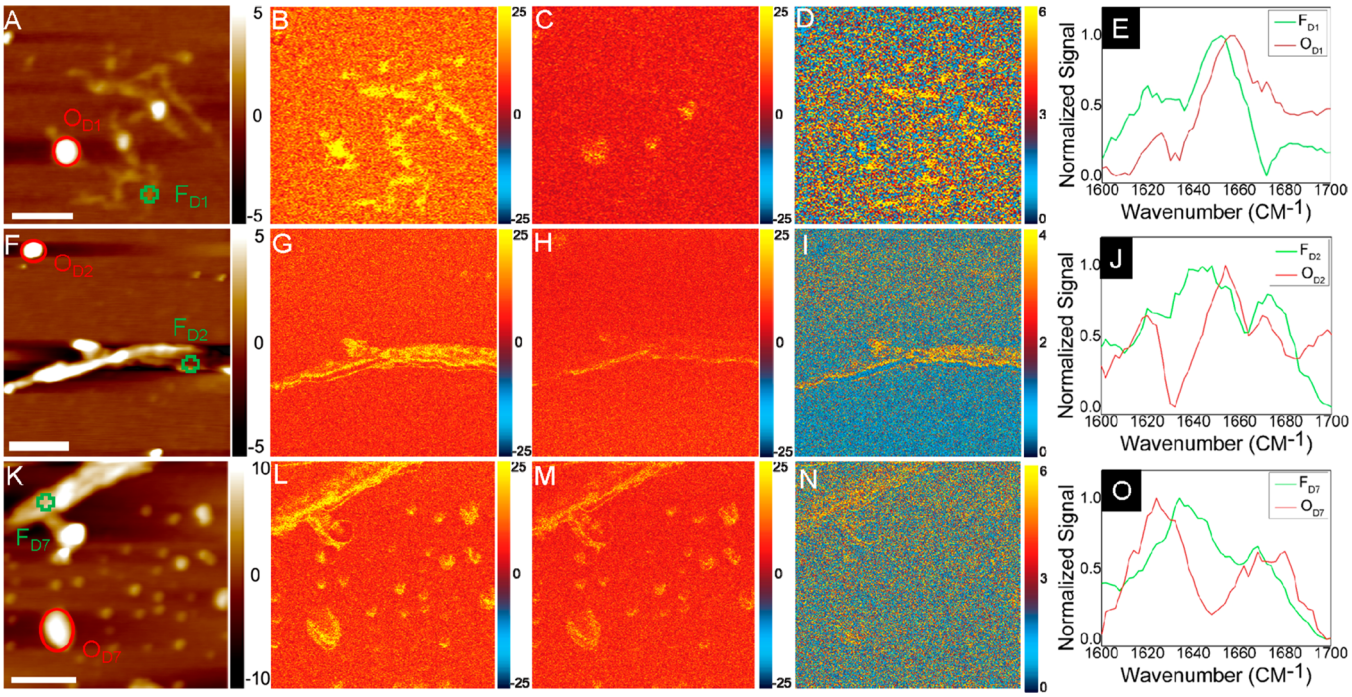

Figure 3. AFM-IR chemical maps and spectra of α-synuclein proteins of D1, D2, and D7. AFM height images (A, F, K), IR absorption map at 1624 cm^{-1} (B, G, L), 1695 cm^{-1} (C, H, M), IR ratio maps of 1624 cm^{-1}/1695 cm^{-1} (D, I, N), and the representative spectra (E, J, O) at D1, D2, and D7, respectively. Scale bar, 250 nm.

α-synuclein aggregation process and reveal the underlying cause of oligomer neurotoxicity.[18] Our study revealed that structural heterogeneity of α-synuclein oligomers is far more complicated. This heterogeneous nature of the oligomers limits the wide application of traditional analytical methods, such as X-ray crystallography and cryo-EM. Moreover, tedious sample separations, such as lyophilization and electrophoresis are required, in which also low contents of intermediate species will be neglected. In comparison, the AFM-IR technique applied by us is capable of differentiating oligomers with diverse secondary structures in the single-particle level. It should be noted that no sample separation procedure is required before measurement. All of the oligomers can be imaged at the same time, regardless of their concentration difference. Owing to these advantages, we are able to visualize the structural heterogeneity as well as structure distribution in a single oligomer level. We also confirm the antiparallel to parallel β-sheet transformation of spherical oligomers is a key step in the fibril formation process. One can envision that such a structural rearrangement may be critically important to control oligomer toxicity, as oligomers with antiparallel β-sheet structure possessed stronger reactive oxygen species (ROS) production and affect membrane permeability upon binding properties relative to monomers and fibrils.[18]

This study also reflects the power of AFM-IR in structural characterization of small protein aggregates. The smallest oligomer analyzed in our work had a height of only 1 nm, which is much smaller than all protein species[17,25,26] studied to date. It should be pointed out that the typical height of many neurodegenerative malady associated fibrils is around 10 nm, like α-synuclein, Aβ-42. Their early oligomers are even smaller. Thus, higher sensitivity toward the growth investigation of these proteins would be highly desired in AFM-IR research.

CONCLUSIONS

We have successfully used AFM-IR to study the morphologic and structural changes of the α-synuclein protein during the aggregation process as well as the structural evolution. We found that these intermediate species, especially the fibrillar aggregates, undergo an increase in β-sheet content during the fibrilization process. Besides that, the spherical oligomeric species exhibit significant diversity in the secondary structure, which verifies the heterogeneity of the growth process. Moreover, the spherical aggregates species always exhibited a higher antiparallel β-sheet content than the fibrillar ones, which leads us to think about the relationship between this antiparallel β-sheet structure and neurotoxicity. These findings demonstrate that the AFM-IR technique could allow us to study the protein aggregation process under ambient conditions in a label-free manner. Different aggregates species can be analyzed at the same time owing to their nanometer resolution feature, regardless of their difference in concentration, size, and height. These features are essential for the study of protein aggregates because of the high heterogeneity nature of their intermediate species. We believe that this method could be easily applied to other protein species like Aβ-42 in order to get a better understanding of the relationship between their secondary structure and potential neurotoxicity.

EXPERIMENTAL METHODS

Detailed information on the experimental methods can be found in the Supporting Information. The preparation of α-synuclein aggregates in this work was similar to that reported previously by Ruggeri et al.[31] In a typical procedure, α-synuclein (AnaSpec, CA) was incubated at a concentration of 50 μM, in 50 mM Tris buffer, 150 mM NaCl, pH 7.5, and under constant agitation at 300 rpm for 11 days.

https://dx.doi.org/10.1021/acs.analchem.0c00593
Anal. Chem. XXXX, XXX, XXX−XXX

■ ASSOCIATED CONTENT

Supporting Information

The Supporting Information is available free of charge at https://pubs.acs.org/doi/10.1021/acs.analchem.0c00593.

AFM images of D0, D1, D2, D3, and D7 samples; infrared chemical maps at 1624 and 1655 cm^{-1}; ATR-FTIR, CD, and AFM-IR spectra on D0, D1, D2, D3, and D7 samples; and experimental details of sample preparations and characterizations (PDF)

■ AUTHOR INFORMATION

Corresponding Author

Dmitry Kurouski − *Department of Biochemistry and Biophysics and The Institute for Quantum Science and Engineering, Texas A&M University, College Station, Texas 77843, United States;* orcid.org/0000-0002-6040-4213; Phone: 979-458-3778; Email: dkurouski@tamu.edu

Author

Lei Zhou − *Department of Biochemistry and Biophysics, Texas A&M University, College Station, Texas 77843, United States*

Complete contact information is available at: https://pubs.acs.org/10.1021/acs.analchem.0c00593

Notes

The authors declare no competing financial interest.

■ ACKNOWLEDGMENTS

The work was supported by the startup funds from Texas A&M University. We would like to thank M. Lasagna for help with the CD measurements.

■ REFERENCES

(1) Dorsey, E. R.; Bloem, B. R. *JAMA Neurol.* **2018**, *75*, 9−10.
(2) Spillantini, M. G.; Schmidt, M. L.; Lee, V. M.-Y.; Trojanowski, J. Q.; Jakes, R.; Goedert, M. *Nature* **1997**, *388*, 839−840.
(3) Glenner, G. G.; Wong, C. W. *Biochem. Biophys. Res. Commun.* **1984**, *120*, 885−890.
(4) DiFiglia, M.; Sapp, E.; Chase, K. O.; Davies, S. W.; Bates, G. P.; Vonsattel, J.; Aronin, N. *Science* **1997**, *277*, 1990−1993.
(5) Eanes, E.; Glenner, G. G. *J. Histochem. Cytochem.* **1968**, *16*, 673−677.
(6) Sunde, M.; Serpell, L. C.; Bartlam, M.; Fraser, P. E.; Pepys, M. B.; Blake, C. C. *J. Mol. Biol.* **1997**, *273*, 729−739.
(7) Jimenez, J. L.; Guijarro, J. I.; Orlova, E.; Zurdo, J.; Dobson, C. M.; Sunde, M.; Saibil, H. R. *EMBO J.* **1999**, *18*, 815−821.
(8) Gremer, L.; Scholzel, D.; Schenk, C.; Reinartz, E.; Labahn, J.; Ravelli, R. B. G.; Tusche, M.; Lopez-Iglesias, C.; Hoyer, W.; Heise, H.; Willbold, D.; Schroder, G. F. *Science* **2017**, *358*, 116−119.
(9) Sipe, J. D.; Cohen, A. S. *J. Struct. Biol.* **2000**, *130*, 88−98.
(10) Kurouski, D.; Dukor, R. K.; Lu, X.; Nafie, L. A.; Lednev, I. K. *Biophys. J.* **2012**, *103*, 522−531.
(11) Jimenez, J. L.; Nettleton, E. J.; Bouchard, M.; Robinson, C. V.; Dobson, C. M.; Saibil, H. R. *Proc. Natl. Acad. Sci. U. S. A.* **2002**, *99*, 9196−9201.
(12) Cremades, N.; Cohen, S. I.A.; Deas, E.; Abramov, A. Y.; Chen, A. Y.; Orte, A.; Sandal, M.; Clarke, R. W.; Dunne, P.; Aprile, F. A.; Bertoncini, C. W.; Wood, N. W.; Knowles, T. P.J.; Dobson, C. M.; Klenerman, D. *Cell* **2012**, *149*, 1048−1059.
(13) Winner, B.; Jappelli, R.; Maji, S. K.; Desplats, P. A.; Boyer, L.; Aigner, S.; Hetzer, C.; Loher, T.; Vilar, M.; Campioni, S.; Tzitzilonis, C.; Soragni, A.; Jessberger, S.; Mira, H.; Consiglio, A.; Pham, E.; Masliah, E.; Gage, F. H.; Riek, R. *Proc. Natl. Acad. Sci. U. S. A.* **2011**, *108*, 4194−4199.
(14) Benilova, I.; Karran, E.; De Strooper, B. *Nat. Neurosci.* **2012**, *15*, 349−357.
(15) Hong, D.-P.; Fink, A. L.; Uversky, V. N. *J. Mol. Biol.* **2008**, *383*, 214−223.
(16) Qi, Z.; Wu, M.; Fu, Y.; Huang, T.; Wang, T.; Sun, Y.; Feng, Z.; Li, C. *Cell. Physiol. Biochem.* **2017**, *44*, 618−633.
(17) Ruggeri, F.; Longo, G.; Faggiano, S.; Lipiec, E.; Pastore, A.; Dietler, G. *Nat. Commun.* **2015**, *6*, 7831.
(18) Chen, S. W.; Drakulic, S.; Deas, E.; Ouberai, M.; Aprile, F. A.; Arranz, R.; Ness, S.; Roodveldt, C.; Guilliams, T.; De-Genst, E. J.; Klenerman, D.; Wood, N. W.; Knowles, T. P.J.; Alfonso, C.; Rivas, G.; Abramov, A. Y.; Valpuesta, J. M.; Dobson, C. M.; Cremades, N. *Proc. Natl. Acad. Sci. U. S. A.* **2015**, *112*, E1994−E2003.
(19) Lorenzen, N.; Nielsen, Sør. B.; Buell, A. K.; Kaspersen, Jør. Døv.; Arosio, P.; Vad, B. S.; Paslawski, W.; Christiansen, G.; Valnickova-Hansen, Z.; Andreasen, M.; Enghild, J. J.; Pedersen, J. S.; Dobson, C. M.; Knowles, T. P. J.; Otzen, D. E. *J. Am. Chem. Soc.* **2014**, *136*, 3859−3868.
(20) Paslawski, W.; Andreasen, M.; Nielsen, S. B.; Lorenzen, N.; Thomsen, K.; Kaspersen, J. D.; Pedersen, J. S.; Otzen, D. E. *Biochemistry* **2014**, *53*, 6252−6263.
(21) Amenabar, I.; Poly, S.; Nuansing, W.; Hubrich, E. H.; Govyadinov, A. A.; Huth, F.; Krutokhvostov, R.; Zhang, L.; Knez, M.; Heberle, J.; Bittner, A. M.; Hillenbrand, R. *Nat. Commun.* **2013**, *4*, 2890.
(22) Henry, S.; Bercu, N.; Bobo, C.; Cullin, C.; Molinari, M.; Lecomte, S. *Nanoscale* **2018**, *10*, 936−940.
(23) Ruggeri, F.; Vieweg, S.; Cendrowska, U.; Longo, G.; Chiki, A.; Lashuel, H.; Dietler, G. *Sci. Rep.* **2016**, *6*, 31155.
(24) Dazzi, A.; Prater, C. B. *Chem. Rev.* **2017**, *117*, 5146−5173.
(25) Rizevsky, S.; Kurouski, D. *ChemBioChem* **2020**, *21*, 481.
(26) Ramer, G.; Ruggeri, F. S.; Levin, A.; Knowles, T. P.; Centrone, A. *ACS Nano* **2018**, *12*, 6612−6619.
(27) Farber, C.; Wang, R.; Chemelewski, R.; Mullet, J.; Kurouski, D. *Anal. Chem.* **2019**, *91*, 2472−2479.
(28) Felts, J. R.; Kjoller, K.; Lo, M.; Prater, C. B.; King, W. P. *ACS Nano* **2012**, *6*, 8015−8021.
(29) Liu, Y.; Collins, L.; Proksch, R.; Kim, S.; Watson, B. R.; Doughty, B.; Calhoun, T. R.; Ahmadi, M.; Ievlev, A. V.; Jesse, S.; Retterer, S. T.; Belianinov, A.; Xiao, K.; Huang, J.; Sumpter, B. G.; Kalinin, S. V.; Hu, B.; Ovchinnikova, O. S. *Nat. Mater.* **2018**, *17*, 1013−1019.
(30) Yoneda, J. S.; Miles, A. J.; Araujo, A. P. U.; Wallace, B. A. *Protein Sci.* **2017**, *26*, 718−726.
(31) Ruggeri, F. S.; Adamcik, J.; Jeong, J. S.; Lashuel, H. A.; Mezzenga, R.; Dietler, G. *Angew. Chem., Int. Ed.* **2015**, *54*, 2462−2466.

https://dx.doi.org/10.1021/acs.analchem.0c00593
Anal. Chem. XXXX, XXX, XXX−XXX